SAND2021-15141C

Study of Titanium Potassium Perchlorate Combustion using Electric Field Holography and Imaging Pyrometry

Andrew W. Marsh*, Gwendolyn T. Wang†, Andy X. Zheng‡, Zachary T. D'Ambra§, Taylor D. Hampson ¶ and Yi Chen Mazumdar‖
Georgia Institute of Technology, Atlanta, GA, 30332, USA

Titanium particles are commonly used in igniters and pyrotechnics to improve combustion performance. Understanding particle kinetics and dynamics in these systems is vital to improving their functionality and preventing accident scenarios. Despite their importance, most prior published studies focus on isolated titanium particle combustion experiments. In this work, we aim to study *in-situ* titanium particle combustion statistics in Ti/$KClO_4$ pyrotechnic igniters. To achieve this, we use simultaneous electric field holography, which captures undistorted three-dimensional holograms of the particle field during combustion, and split-image two-color pyrometry, which estimates projected titanium particle surface temperatures. Here, we discuss the measurement theory, present preliminary experimental results, and describe measurement statistics in order to show the feasibility of these diagnostics for studying *in-situ* titanium particle combustion in extreme pyrotechnic environments.

I. Introduction

METAL particles are common components in many energetic mixtures including solid fuels [1, 2], pyrotechnics [3–5], and explosives [6, 7]. Due to their high energy density [8] and high peak flame temperatures [9], metals such as titanium are often used in energetic materials to improve combustion characteristics. During the combustion and oxidation processes of titanium particles, a TiO_2 film builds up on the surface. Underneath this film, the molten Ti begins to cool and solidify. At the same time, gas forms near the center and causes pressure to build up within the particle, eventually resulting in fragmentation and dispersal of smaller titanium particles [9, 10]. Understanding the particle sizes, velocities, and temperatures of titanium particles during this combustion process is important not only for assessing the performance of existing formulations but also for future energetic materials development.

Titanium combustion has been previously studied using high-speed videography [10], single-point three color pyrometry [11], and spectroscopy [12]. However, many of these past studies have focused on isolated titanium particle combustion in controlled environments; there is little work on titanium particle combustion dynamics *in-situ* to igniter or pyrotechnic systems [13]. Additionally, due to high particle velocities, shock-waves, and focal depth limitations, many existing diagnostics are not suitable for studying titanium particle combustion. Finally, there is a lack of spatially resolved temperature measurements, as most prior work focuses on single point diagnostics [11, 12]. To better understand titanium particle combustion in these extreme systems with significant optical distortions, new spatially and temporally resolved diagnostics are needed.

In this paper, we investigate titanium particle combustion characteristics in a Ti/$KClO_4$ pyrotechnic formulation, commonly used for thermal battery ignition [14]. To accomplish this, we use simultaneous phase shifting electric field holography and split-image two-color pyrometry to capture size, velocity, and temperature measurements of these particles at various heights above the igniter surface. While simultaneous holography and pyrometry has been performed on aluminum particles in solid propellant in the past [15–20], these techniques have not been used to study titanium particle combustion. Holography, which is capable of capturing three-dimensional particle field information on a two-dimensional sensor, is not focal depth limited because it operates by numerically refocusing diffraction patterns. This allows for a higher quantity of particles to be segmented and studied from a single ignition experiment [15, 16, 21–24]. Since significant phase distortions from flame zones and temperature gradients are present, distortion cancelling forms

*Ph.D. Student, Woodruff School of Mechanical Engineering, amarsh32@gatech.edu
†Ph.D. Student, Woodruff School of Mechanical Engineering, gtwang@gatech.edu
‡Ph.D. Student, Woodruff School of Mechanical Engineering, azheng36@gatech.edu
§Undergraduate Researcher, Guggenheim School of Aerospace Engineering, zdambra3@gatech.edu
¶Undergraduate Researcher, Guggenheim School of Aerospace Engineering, tdhampson12@gatech.edu
‖Assistant Professor, Woodruff School of Mechanical Engineering, ellen.mazumdar@me.gatech.edu, Member AIAA.

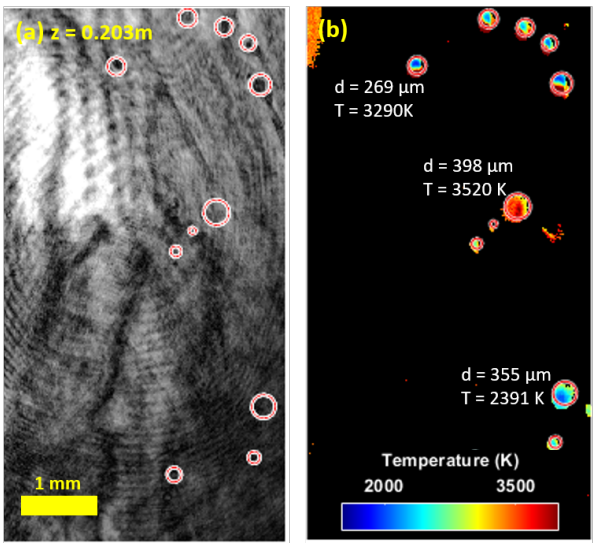

Fig. 1 A simultaneous (a) phase shifted electric field hologram refocused in the z-direction to a plane containing particles and (b) a corresponding temperature field from pyrometry.

of holography [25–28] are needed instead of traditional digital inline holography (DIH) techniques. Using the spatial information from the distortion-cancelling form of electric field holography [25, 27], particle locations can be identified and later used to help extract temperature measurements from a ratio of pyrometry images captured at two different wavelengths [29, 30], as shown in Fig. 1(b). This combination of diagnostics provides joint spatial and temperature statistics for the titanium particles, enabling the study of these particles as they proceed through the combustion processes.

II. Experimental Techniques

In this work, an uncapped, stoichiometric mixture of sponge-Ti/$KClO_4$ (32% w.t. Ti, 68% w.t. $KClO_4$) is used to study metal particle combustion. This mixture is commonly used for secondary ignition of non-stoichiometric Fe/$KClO_4$ thermal heat pellets [31], where the titanium particle combustion characteristics are thought to be the major driver in the ignition performance of the pellets. In order to better understand the physics that drive this ignition process, the size, velocity, and temperature statistics of the titanium particles need to be investigated above the igniter. To study these titanium particles, we use a simultaneous phase shifting electric field holography technique and a split-image two-color pyrometry diagnostic, as shown in Fig. 2. Holography retrieves spatial information while pyrometry provides surface temperature estimates.

For the electric field holography diagnostic, a continuous 532 nm laser (Photonics Industries DS20-532, 20W) is expanded and collimated before separating into two beams. One leg passes through the field containing the objects of interest while the other leg, which functions as the reference beam, passes through a half-wave plate to rotate the light polarization. The two beams are then recombined and magnified by a long distance microscope to maintain an adequate standoff from the igniter. Finally, the beam passes through a quarter waveplate to circularly polarize the light, which is projected onto the camera. Here, the high-speed polarization camera (Photron Crysta Pl-1P, 7000 fps at full frame, 12-bit depth, 1024×1024 pixels, pixel size of 20 μm) contains on-chip wire-grid polarizers on each pixel to generate four polarized images (at 0, $\pi/2$, π, and $3\pi/2$) of the same object.

At the same time, light emitting from the hot titanium particles travels through a lens and through two knife blades at the focal point to create an image with sharp edges that is half the size of the pyrometry camera's sensor. The light subsequently passes through another lens and split into two legs using a dichroic mirror and filters to isolate two specific wavelengths at 750 and 850 nm. Each leg is retro-reflected to ensure both legs to come into focus in the same plane. Finally, the two pyrometry images appear side-by-side on a single camera sensor without image overlap. For imaging pyrometry, we use a high-speed Photron SA 1.1 (5400 fps at full frame, 12-bit depth, 1024×1024 pixels, pixel size of 20 μm).

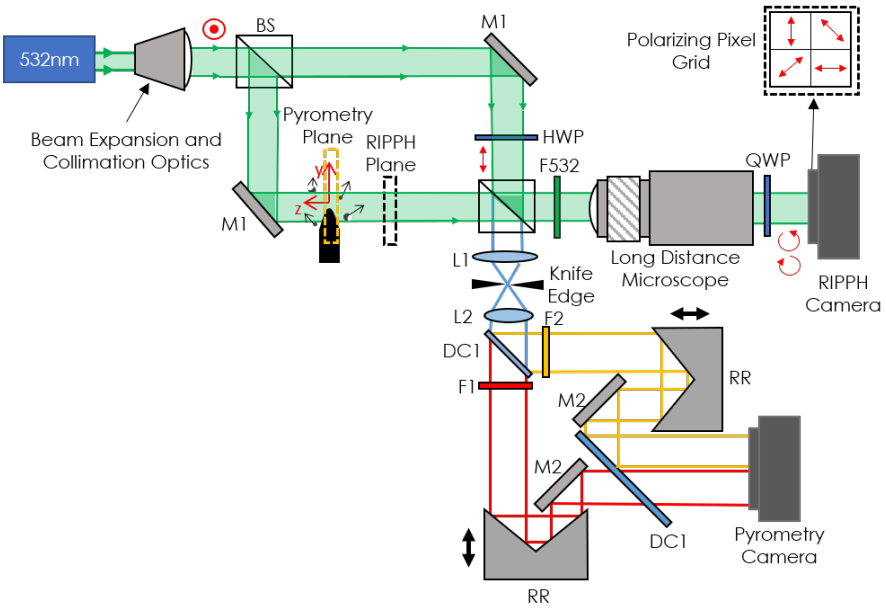

Fig. 2 The experimental setup for simultaneous polarization phase shifting electric field holography and split-image two-color pyrometry is shown. BS - 50/50 beam splitter, M1 - 532 nm laser-line mirror, M2 - broadband mirror, HWP - half wave plate, QWP - quarter wave plate, L1 - AF-S Nikkor 85 mm f/18.G, L2 - AF-S DX Nikkor 55 mm f/1.8G, DC1 - dichroic longpass 805 nm, RR - retroreflector, F532 - 532 nm filter 10 nm FWHM (full width at half maximum), F1 - 850 nm filter 10 nm FWHM, F2 - 750 nm filter 10 nm FWHM.

A. Electric Field Holography

In digital holography, a collimated beam passes through an object field in order to capture diffraction images generated by the particles. The resulting holograms can be numerically refocused using the diffraction integral equation. Digital inline holography (DIH) is a simple and robust form of holography that has been applied extensively to multiphase flows [21, 24]. In DIH, no reference beam is present and the diffraction patterns are numerically refocused using,

$$E_h(x, y, z) = [I_h(x, y) \cdot R^*(x, y)] \otimes g(x, y, z), \tag{1}$$

where I_h is the image intensity, R^* is the the conjugate of the planar reference wave approximated as 1, and g is the diffraction kernel [25, 26]. Since DIH is self-referenced, phase estimates are not available. This leaves DIH vulnerable to phase delay distortions from index of refraction gradients, which can be caused by shock waves and flame zones that can severely distort the hologram.

In order to retrieve both amplitude and phase information to construct an undistorted hologram, we use phase

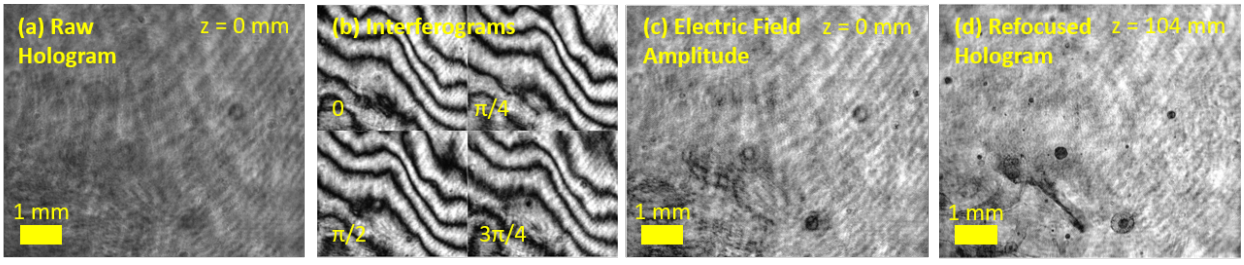

Fig. 3 (a) The raw hologram captured using the polarization camera can be split into (b) four $\pi/4$ shifted interferograms. (c) The interferograms are used to reconstruct the electric field containing both amplitude and phase information. This electric field can then be numerically refocused to obtain (d) an undistorted, in focus hologram of the titanium particles.

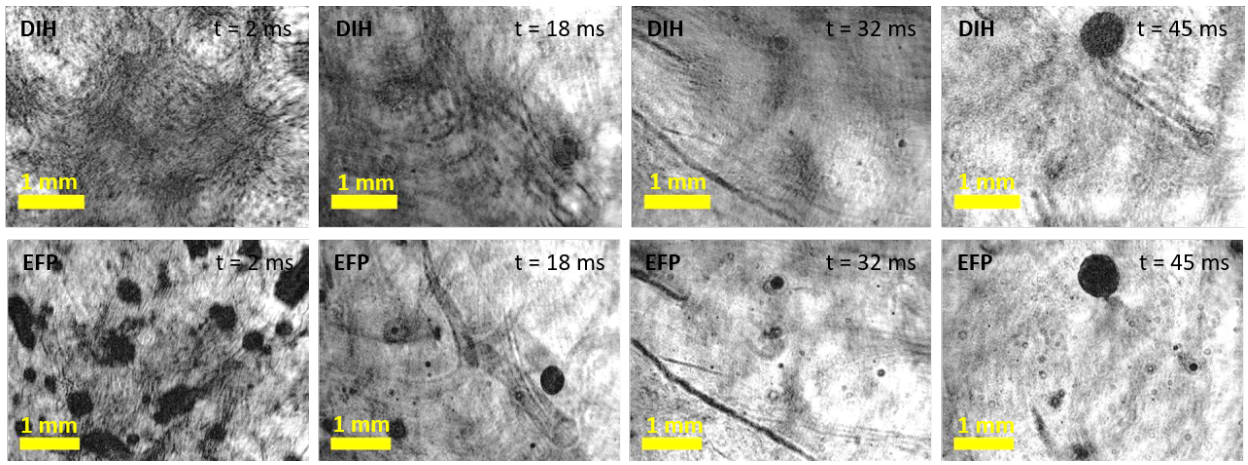

Fig. 4 Comparison of digital inline holography to electric field propagation for Ti/$KClO_4$ combustion. DIH shows significant phase distortions early in the combustion process that are corrected using EFP.

shifting electric field propagation (EFP) phase holography instead. Here, four $\frac{\pi}{2}$ shifted interferograms (I_0, $I_{\frac{\pi}{2}}$, I_π, and $I_{\frac{3\pi}{2}}$) are produced by extracting polarized images from the camera data. Then, 2D-cubic interpolation is applied to fill in missing pixels and produce four full-resolution interferograms, as shown in Fig. 3(b). The reconstructed electric field is,

$$O(x,y) = \frac{1}{4A_r}\left[(I_0 - I_\pi) + i\left(I_{\frac{\pi}{2}} - I_{\frac{3\pi}{2}}\right)\right], \tag{2}$$

where A_r is the amplitude of the electric field. This electric field hologram contains both amplitude information (shown in Fig. 3(c)) and phase information and can be refocused to new z-planes using $E_E(x,y,z) = (O(x,y)\cdot R^*(x,y)) \otimes g(x,y,z)$. Since this technique contains relative phase information propagated from the image plane to other z-planes, fewer phase distortions occur, resulting in a more accurate image. Although applying electric field holography methods remove the majority of phase distortions, additional phase distortions still remain. These residual distortions can be removed at the distortion plane by further applying a recalculated intensity propagation phase holography technique [25, 27].

B. Split-Image Pyrometry

To estimate particle surface temperatures using a single high-speed camera, we utilize a split-image two-color imaging pyrometer configuration. Here, 750 and 850 nm wavelengths are selected to avoid emission peaks from the igniter, as shown in Fig. 5. Wavelengths below 500 nm were not used in this study but can potentially be applied in

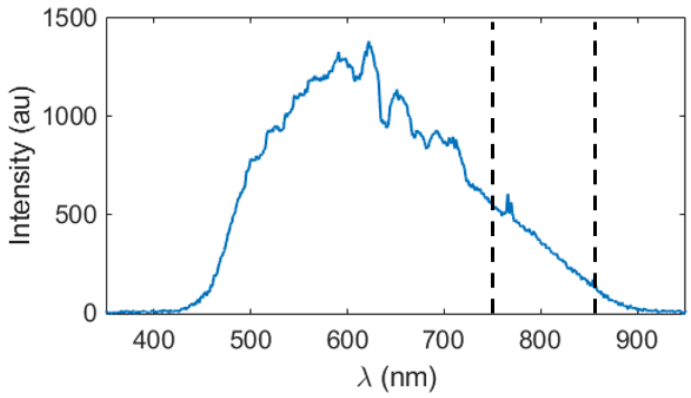

Fig. 5 Experimental emission spectrum of Ti/$KClO_4$ combustion. Dashed lines at 750 nm and 850 nm indicate locations in the spectrum that are free from emission peaks, which are used for two-color pyrometry.

future work. In order to balance the dynamic range in both legs of the pyrometer, an OD 0.6 neutral density filter was added to the 750 nm leg.

Temperatures for each pixel can be extracted from the two pyrometry images by assuming gray-body emission for the titanium particles. By using Wien's approximation for Plank's law, the pixel intensity can be approximated as,

$$I_w(T,\lambda) = (2hc^2\epsilon/\lambda^5)e^{-hc/\lambda kT}, \tag{3}$$

where I_w is the pixel intensity, h is Planck's constant, c is the speed of light, λ is the wavelength, and k is the Boltzmann constant. The ratio of the intensities at the two wavelengths is,

$$\Gamma = (I_2\eta_1\zeta_1)/(I_1\eta_2\zeta_2), \tag{4}$$

where η is the camera and filter efficiency and ζ is the exposure duration. We neglect the camera exposure term since both images are captured with the same exposure on the same camera. The ratio Γ can then be used to find the temperature in each pixel using,

$$T_w = \left[\frac{k}{hc}\frac{\lambda_1\lambda_2}{\lambda_2-\lambda_1}\left(\ln(\Gamma) - 5\ln\left(\frac{\lambda_1}{\lambda_2}\right)\right)\right]^{-1}. \tag{5}$$

Two-color pyrometer simulations, found by calculating the black body emissions at the expected experimental temperature range, are shown in Fig. 6(a). To find the emitted intensity that the camera perceives, as shown in Fig. 6(b), the quantum efficiency of the camera must be applied to the emission curves. This intensity is then scaled to a 12-bit depth where the lowest intensity is assigned 0 and the highest intensity is assigned to the max bit value in order to represent the camera output. With camera bit values and the associated temperatures, temperature measurement resolution analysis was conducted by determining the change in temperature associated with the minimum change in intensity ratio. The minimum change in the intensity ratio was then determined by adding one bit to the lower intensity of the ratio. For example, at a bit depth of 1000 for the 750 nm intensity, the temperature resolution was found to be 1.9 K; this value decreases as the intensity increases.

Next, the split-image pyrometer was calibrated against a commercial single point two-color pyrometer (Process Sensors Corp. Metis M311, 1000 to 3000 °C temperature range, 870 and 990 nm wavelengths) while simultaneously measuring the temperature of a tungsten lamp at varying temperatures. With this method, calibrating the imaging pyrometer does not require moving the setup to a high temperature black-body source [15]. Using this calibration technique, the 750 nm and 850 nm images, shown in Fig. 6(c-d), are ratioed to obtain the temperature map shown in Fig. 6(e).

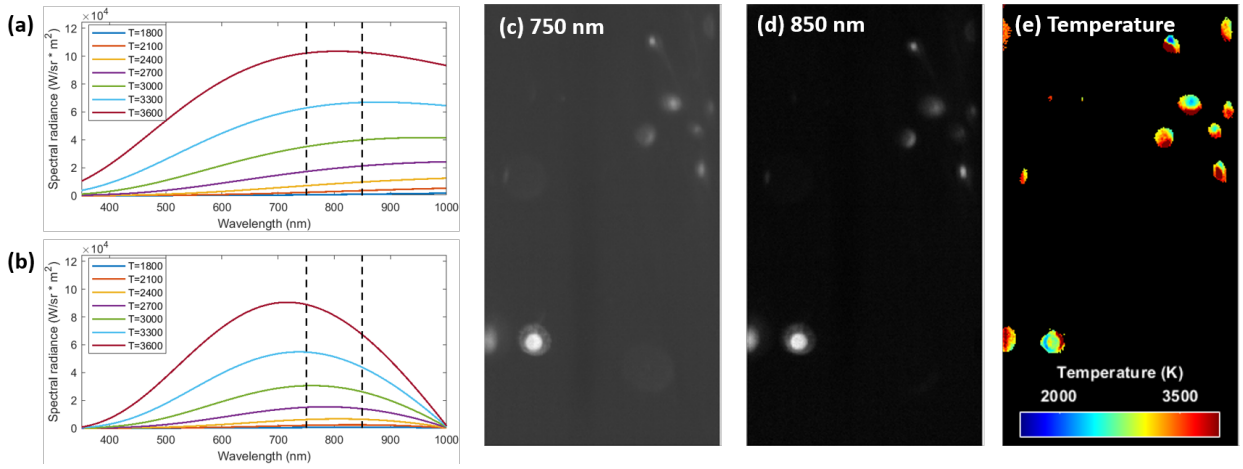

Fig. 6 (a) The simulated blackbody radiation curve and (b) the same curve accounting for the camera quantum efficiency. By taking the ratio of (c) the 750 nm and (d) 850 nm images and applying the Wien's approximation, the (e) temperature map can be calculated.

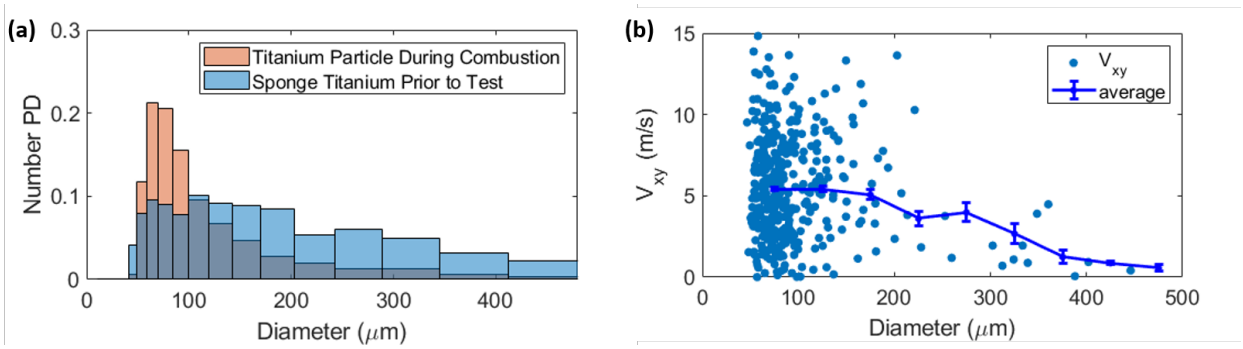

Fig. 7 (a) Size distributions of the sponge titanium particles before combustion compared to the measured diameter during combustion are shown. (b) Velocity distribution of the titanium particles are also illustrated with standard error bars.

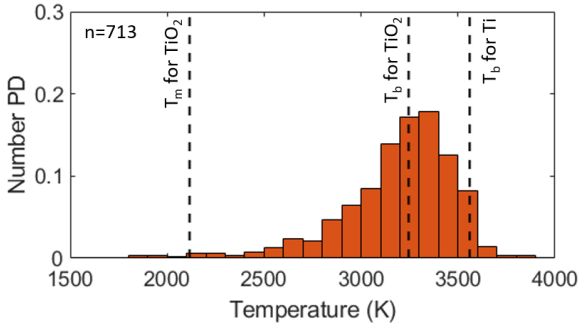

Fig. 8 The temperature distribution of the titanium particles show that the majority of temperatures fall between the melting point of TiO_2 and boiling point of TiO_2 and Ti.

III. Results

Particle statistics were collected from four uncapped 30 mg Ti/$KClO_4$ samples in which the combustion process lasted a duration of ~80 ms each. From these four samples, the holography image segmentation algorithm identified 1975 titanium particle tracks, of which 713 were within the pyrometry image field-of-view limits. Qualitatively, the holography data shows higher particle densities early in the combustion process that steeply drops off as the process continues, as shown in Fig. 4. The majority of particles in these experiments are contained within the smoke cloud while a handful of small, fast particles are ejected in front of the smoke cloud.

For the spatial statistics, only particles that were between ±10 mm of the center of the igniter were tracked. The minimum detectable particle size for these experiments was 45 μm, which is controlled by the magnification and the pixel size. The size distribution statistics reveal a high number of small particles (<100 μm in diameter) and a smaller number of larger diameter particles, as shown in Fig. 7(a). In comparison, the number probability density of the sponge titanium particle diameters prior to combustion show a larger quantity of larger diameter particles. This result could indicate that there is little particle agglomeration, potentially due to the rapid nature of the combustion process that ejects particles into the air. In Fig. 7(b), the measured velocity of the particles appears to be driven by drag, as the rapid expansion of gas within the igniter cup forces the particles upward into the air. This results in smaller particles having higher velocities around 5 m/s while larger particles have lower velocities.

Next, the titanium particle surface temperature distribution, illustrated in Fig. 8, is analyzed. Here, the majority of projected particle surface temperatures fall between the melting point of TiO_2 and the boiling point of Ti or TiO_2. Due to the morphology of titanium particles having a homogeneous TiO_2 surface, most of the surface temperatures should be below the boiling point of TiO_2. For these results, the temperature measurements may be biased toward higher temperatures both due to the nature of the nonlinearities associated with pyrometry measurement process and slight offsets in image alignment. While these results present interesting surface temperature data for *in-situ* titanium combustion, additional work is still needed to actively quantify and minimize uncertainties.

IV. Conclusions

In this paper, uncapped sponge-Ti/$KClO_4$ igniters are studied to better understand the *in-situ* combustion of titanium particles. This is done by measuring and analyzing the size, velocity, and temperature statistics of titanium particles during combustion from 30 mg samples of stoichiometric Ti/$KClO_4$ at a height of 19 to 27 mm above the igniter. To accomplish this, electric field holography is used to measure spatial characteristics and split-image pyrometry is used to measure surface temperatures. Results showed no significant change in the particle size before and during to combustion, which potentially indicates minimal particle agglomeration of the titanium particles. Velocity distributions showed that smaller velocities were ejected at higher velocities than larger particles. Finally, the particle temperature distribution indicates that the majority of surface temperatures falling between the melting point of TiO_2 and the boiling point of Ti and TiO_2.

Ultimately, this work provides a unique preliminary analysis of titanium particle combustion by demonstrating measurements of a statistically significant number of particles during the combustion of a pyrotechnic igniter. Results from this study and future follow-on experiments will help improve our understanding of titanium particle combustion in previously understudied pyrotechnic igniter systems .

Acknowledgments

The authors would like to thank Sean Kearney, Benjamin Halls, Ryan Marinis, and Shawn Stacy from Sandia National Labs for their invaluable insight on pyrotechnic igniters. Support from the Sandia National Laboratories Academic Alliance Laboratory Directed Research and Development (LDRD) program is gratefully acknowledged. Sandia National Laboratories is a multimission laboratory managed and operated by National Technology and Engineering Solutions of Sandia, LLC., a wholly owned subsidiary of Honeywell International, Inc., for the U.S. Department of Energy's National Nuclear Security Administration under contract DE-NA0003525. The views expressed in the article do not necessarily represent the views of the U.S. Department of Energy or the United States Government.

References

[1] Gany, A., and Netzer, D., "Combustion Studies of Metallized Fuels for Solid-Fuel Ramjets," *J. Propulsion*, Vol. 2, No. 5, 1986, pp. 423–427.

[2] Melcher, J. C., Krier, H., and Burton, R. L., "Burning Aluminum Particles Inside a Laboratory-Scale Solid Rocket Motor," *Journal of Propulsion and Power*, Vol. 18, No. 3, 2002, pp. 631–640. https://doi.org/10.2514/2.5977.

[3] Lee, J.-S., Lin, L.-K., Huang, P.-J., Chen, S.-Y., and Ch'en, P.-J., "Thermal Behaviour and Firing Characteristics of Zr/KClO4 Primer Mixture Containing Different Particle Sizes of Zirconium," *Thermochimica Acta*, Vol. 181, 1991, pp. 329–336.

[4] Miyata, K., and Kubota, N., "Combustion of Ti and Zr Particles with KNO3," *Propellants, Explosives, Pyrotechnics*, Vol. 21, No. 1, 1996, pp. 29–35. https://doi.org/10.1002/prep.19960210107.

[5] Wang, H., Kline, D. J., Biswas, P., and Zachariah, M. R., "Connecting Agglomeration and Burn Rate in a Thermite Reaction: Role of Oxidizer Morphology," *Combustion and Flame*, Vol. 231, 2021, p. 111492. https://doi.org/10.1016/j.combustflame.2021.111492.

[6] Mao, X., Jiang, L., Zhu, C., and Wang, X., "Effects of Aluminum Powder on Ignition Performance of RDX, HMX, and CL-20 Explosives," *Advances in Materials Science and Engineering*, Vol. 2018, 2018, pp. 1–8. https://doi.org/10.1155/2018/5913216.

[7] Gottfried, J. L., Smith, D. K., Wu, C.-C., and Pantoya, M. L., "Improving the Explosive Performance of Aluminum Nanoparticles with Aluminum Iodate Hexahydrate (AIH)," *Scientific Reports*, Vol. 8, No. 1, 2018. https://doi.org/10.1038/s41598-018-26390-9.

[8] Bergthorson, J., Goroshin, S., Soo, M., Julien, P., Palecka, J., Frost, D., and Jarvis, D., "Direct Combustion of Recyclable Metal Fuels for Zero-carbon Heat and Power," *Applied Energy*, Vol. 160, 2015, pp. 368–382. https://doi.org/10.1016/j.apenergy.2015.09.037.

[9] Glotov, O. G., "Ignition and Combustion of Titanium Particles: Experimental Methods and Results," *Physics-Uspekhi*, Vol. 62, No. 2, 2019, pp. 131–165. https://doi.org/10.3367/ufne.2018.04.038349.

[10] Shafirovich, E., Teoh, S. K., and Varma, A., "Combustion of Levitated Titanium Particles in Air," *Combustion and Flame*, Vol. 152, No. 1-2, 2008, pp. 262–271. https://doi.org/10.1016/j.combustflame.2007.05.008.

[11] Molodetsky, I., "Phases of Titanium Combustion in Air," *Combustion and Flame*, Vol. 112, No. 4, 1998, pp. 522–532. https://doi.org/10.1016/s0010-2180(97)00146-6.

[12] Badiola, C., and Dreizin, E. L., "Combustion of Micron-sized Particles of Titanium and Zirconium," *Proceedings of the Combustion Institute*, Vol. 34, No. 2, 2013, pp. 2237–2243. https://doi.org/10.1016/j.proci.2012.05.089.

[13] LoCurto, A. C., Welch, M. A., Sippel, T. R., and Michael, J. B., "High-speed Visible Supercontinuum Laser Absorption Spectroscopy of Metal Oxides," *Optics Letters*, Vol. 46, No. 13, 2021, pp. 3288–3291. https://doi.org/10.1364/OL.428456.

[14] Guidotti, R. A., Odinek, J., and Reinhardt, F. W., "Characterization of Fe/KClO4 Heat Powders and Pellets," *Journal of Energetic Materials*, Vol. 24, No. 4, 2006, pp. 271–305. https://doi.org/10.1080/07370650600896566.

[15] Chen, Y., Guildenbecher, D. R., Hoffmeister, K. N., Cooper, M. A., Stauffacher, H. L., Oliver, M. S., and Washburn, E. B., "Study of Aluminum Particle Combustion in Solid Propellant Plumes using Digital In-line Holography and Imaging Pyrometry," *Combustion and Flame*, Vol. 182, 2017, pp. 225–237. https://doi.org/10.1016/j.combustflame.2017.04.016.

[16] Powell, M. S., Gunduz, I. W., Shang, W., Chen, J., Son, S. F., Chen, Y., and Guildenbecher, D. R., "Agglomerate Sizing in Aluminized Propellants Using Digital Inline Holography and Traditional Diagnostics," *Journal of Propulsion and Power*, Vol. 34, No. 4, 2018, pp. 1002–1014. https://doi.org/10.2514/1.b36859.

[17] Chen, Y., Heyborne, J. D., and Guildenbecher, D. R., "Time-resolved Digital In-line Holography and Pyrometry for Aluminized Solid Rocket Propellants," *OSA Imaging and Applied Optics Conference: Laser Applications to Chemical, Security and Environmental Analysis*, 2018, p. LTu3C.5. https://doi.org/10.1364/LACSEA.2018.LTu3C.5.

[18] Chen, Y., Guildenbecher, D. R., Hoffmeister, K. N., and Sojka, P. E., "Digital Imaging Holography and Pyrometry of Aluminum Drop Combustion in Solid Propellant Plumes," *OSA Imaging and Applied Optics Conference: Laser Applications to Chemical, Security and Environmental Analysis*, 2016, p. LT4F.2. https://doi.org/10.1364/LACSEA.2016.LT4F.2.

[19] Marsh, A. W., Wang, G. T., Heyborne, J. D., Guildenbecher, D. R., and Mazumdar, Y. C., "Time-resolved Size, Velocity, and Temperature Statistics of Aluminum Combustion in Solid Rocket Propellants," *Proceedings of the Combustion Institute*, Vol. 38, No. 3, 2021, pp. 4417–4424. https://doi.org/10.1016/j.proci.2020.08.010.

[20] Marsh, A. W., Zheng, A. X., Heyborne, J. D., Guildenbecher, D. R., and Mazumdar, Y. C., "Solid Propellant Scaling Analysis Using Simultaneous Holography and Imaging Pyrometry," *59h AIAA Aerospace Sciences Meeting*, 2021, pp. AIAA 2021–1373. https://doi.org/10.2514/6.2021-1373.

[21] Chen, Y., Wagner, J. L., Farias, P. A., DeMauro, E. P., and Guildenbecher, D. R., "Galinstan Liquid Metal Breakup and Droplet Formation in a Shock-induced Cross-flow," *International Journal of Multiphase Flow*, Vol. 106, 2018, pp. 147–163. https://doi.org/10.1016/j.ijmultiphaseflow.2018.05.015.

[22] Sheng, J., Malkiel, E., and Katz, J., "Using Digital Holographic Microscopy for Simultaneous Measurements of 3D Near Wall Velocity and Wall Shear Stress in a Turbulent Boundary Layer," *Experiments in Fluids*, Vol. 45, No. 6, 2008, pp. 1023–1035. https://doi.org/10.1007/s00348-008-0524-2.

[23] Guildenbecher, D. R., Wagner, J. L., Olles, J. D., Demauro, E. P., Farias, P., Grasser, T. W., and Sojka, P. E., "kHz Rate Digital In-line Holography Applied to Quantify Secondary Droplets from the Aerodynamic Breakup of a Liquid Column in a Shock-Tube," *54th AIAA Aerospace Sciences Meeting*, American Institute of Aeronautics and Astronautics, 2016. https://doi.org/10.2514/6.2016-1044.

[24] Katz, J., and Sheng, J., "Applications of Holography in Fluid Mechanics and Particle Dynamics," *Annual Review of Fluid Mechanics*, Vol. 42, No. 1, 2010, pp. 531–555. https://doi.org/10.1146/annurev-fluid-121108-145508.

[25] Marsh, A. W., Evans, T. M., Musci, B., Uzodima, J., Kearney, S. P., Guildenbecher, D. R., and Mazumdar, Y. C., "Phase Distortion Cancellation Using Recalculated Intensity Propagation Phase Holography," *Optics and Lasers in Engineering*, 2021.

[26] Mazumdar, Y. C., Smyser, M. E., Heyborne, J. D., Slipchenko, M. N., and Guildenbecher, D. R., "Megahertz-rate Shock-wave Distortion Cancellation via Phase Conjugate Digital In-line Holography," *Nature Communications*, Vol. 11, 2020, p. 1129. https://doi.org/10.1038/s41467-020-14868-y.

[27] Evans, T. M., Marsh, A. W., Uzodinma, J., Guildenbecher, D. R., and Mazumdar, Y. C., "Digital Phase-Sensitive Holography for Numerical Shock-wave Distortion Cancellation," *58th AIAA Aerospace Sciences Meeting*, 2020, pp. AIAA 2020–1972. https://doi.org/10.2514/6.2020-1972.

[28] Chen, Y., Heyborne, J. D., Guildenbecher, D. R., Smyser, M. E., and Slipchenko, M. N., "Ultra-high-speed Pulse-burst Phase Conjugate Digital In-line Holography for Imaging Through Shock-wave Distortions," *57th AIAA Aerospace Sciences Meeting*, 2019, pp. AIAA 2019–1602. https://doi.org/10.2514/6.2019-1602.

[29] Panagiotou, T., Levendis, Y., and Delichatsios, M., "Measurements of Particle Flame Temperatures using Three-color Optical Pyrometry," *Combustion and Flame*, Vol. 104, No. 3, 1996, pp. 272–287. https://doi.org/10.1016/0010-2180(95)00119-0.

[30] Brazyn, T., Krier, H., and Glumac, N., "Combustion of Nanoaluminum at Elevated Pressure and Temperature Behind Reflected Shock Waves," *Combustion and Flame*, Vol. 145, No. 4, 2006, pp. 703–713. https://doi.org/10.1016/j.combustflame.2005.12.017.

[31] Guidotti, R. A., and Masset, P., "Thermally Activated ("Thermal") Battery Technology," *Journal of Power Sources*, Vol. 161, No. 2, 2006, pp. 1443–1449. https://doi.org/10.1016/j.jpowsour.2006.06.013.